Analogue Implementation of a Fractional-Order PI^{\lambda} Controller for DC Motor Speed Control

HERENCSÁR, N.; KARTCI, A.; KOTON, J.; ŠOTNER, R.; ALAGOZ, A. B.; YEROGLU, C.

Proceedings of the 2019 IEEE 28th International Symposium on Industrial Electronics (ISIE), Vancouver, Canada, pp. 467-472

eISBN: 978-1-7281-3666-0

ISSN: 2163-5145

DOI: https://doi.org/10.1109/ISIE.2019.8781237

Accepted manuscript

Analogue Implementation of a Fractional-Order PI$^{\lambda}$ Controller for DC Motor Speed Control

Norbert Herencsar
Dept. of Telecommunications
Brno University of Technology
Brno, Czech Republic
herencsn@feec.vutbr.cz

Aslihan Kartci
Dept. of Radio Elect. / Telecomm.
Brno University of Technology
Brno, Czech Republic
kartci@feec.vutbr.cz

Jaroslav Koton
Dept. of Telecommunications
Brno University of Technology
Brno, Czech Republic
koton@feec.vutbr.cz

Roman Sotner
Dept. of Radio Electronics
Brno University of Technology
Brno, Czech Republic
sotner@feec.vutbr.cz

Baris Baykant Alagoz
Dept. of Computer Engineering
Inonu University
Malatya, Turkey
baykant.alagoz@inonu.edu.tr

Celaleddin Yeroglu
Dept. of Computer Engineering
Inonu University
Malatya, Turkey
c.yeroglu@inonu.edu.tr

***Abstract*—In this paper, an approach to design a fractional-order integral operator s^{λ} where $-1 < \lambda < 0$, using an analogue technique, is presented. The integrator with a constant phase angle −80.1 degree (i.e. order $\lambda = -0.89$), bandwidth greater than 3 decades, and maximum relative phase error 1.38% is designed by cascade connection of first-order bilinear transfer segments and first-order low-pass filter. The performance of suggested realization is demonstrated in a fractional-order proportional-integral (FOPI$^{\lambda}$) controller described with proportional constant 1.37 and integration constant 2.28. The design specification corresponds to a speed control system of an armature controlled DC motor, which is often used in mechatronic and other fields of control theory. The behavior of both proposed analogue circuits employing two-stage Op-Amps is confirmed by SPICE simulations using TSMC 0.18 µm level-7 LO EPI SCN018 CMOS process parameters with ±0.9 V supply voltages.**

Keywords—fractional calculus, fractional-order integrator, FOPI$^{\lambda}$ controller, DC motor, two-stage Op-Amp

I. INTRODUCTION

Proportional-integral-derivative (PID) controllers are used for more than 90 % of control applications in the industry, because many simple auto-tuning methods and realization techniques for PID controllers are available [1]–[8]. In recent years, the survey [9] indicates fractional-order (FO) controllers become an emerging research topic since they provide many benefits in the control area. This is because the fractional calculus describes the dynamic characteristics of plant more precisely than integer-order description [10]. As Fig. 1 illustrates, the traditional PIDs are a particular case of fractional-order PI$^{\lambda}$D$^{\mu}$ (FOPI$^{\lambda}$D$^{\mu}$) controllers. Hence while design, FO controllers have an additional degrees of freedom and thus offer potential reduction of the control effort, which also results in reduction of wasted energy. Utilization only proportional-integral (PI) controllers is sufficient in wide range of industrial control problems. Although digital controllers are used more often, the role of controllers designed via analogue technique should not be underestimated [8]–[14]. Our brief literature survey indicates various implementation techniques for the fractional-order integral operator s^{λ}, where $-1 < \lambda < 0$ realization in the Laplace domain [15], [16]. A polymer composites or ferroelectric materials-based solid-state elements [17]–[20], approximating impedance with fractional-order character of using passive ladder RC structures [21], emulators using active building blocks [22], or cascade of so-called bilinear transfer segments (BTSs) [23] are among them. Considering the last approach, most often first-order BTS is used, which is a two-port network with a single pole and a single zero. As it is known, the cascade of BTSs creates so-called constant phase block, which generates desired magnitude and phase response by proper setting of both polynomial roots (zero and pole frequencies) of each BTS [24], [25]. Hence, this approach ensures direct emulation of the behavior of a fractional-order integrator (I$^{\lambda}$), which is very beneficial for FOPI$^{\lambda}$ design.

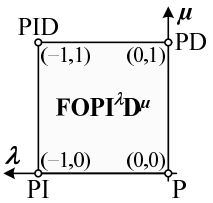

Fig. 1. Generalization of FOPI$^{\lambda}$D$^{\mu}$ controller from points to plane

The main objective of this work is to introduce a new analogue implementation of a FOPI$^{\lambda}$ controller employing Op-Amps. Two-stage Op-Amp implemented in CMOS technology is used, which is a fundamental building block and widely used in analogue integrated circuits and systems. The proposed

This article is based upon support of international mobility project MeMoV, No. CZ.02.2.69/0.0/0.0/16_027/00083710 funded by European Union, Ministry of Education, Youth and Sports, Czech Republic and Brno University of Technology. Research described in this paper is based upon work from COST Action CA15225, a network supported by COST (European Cooperation in Science and Technology) and Ministry of Education, Youth and Sports under grant LTC18022 of Inter-Cost program.

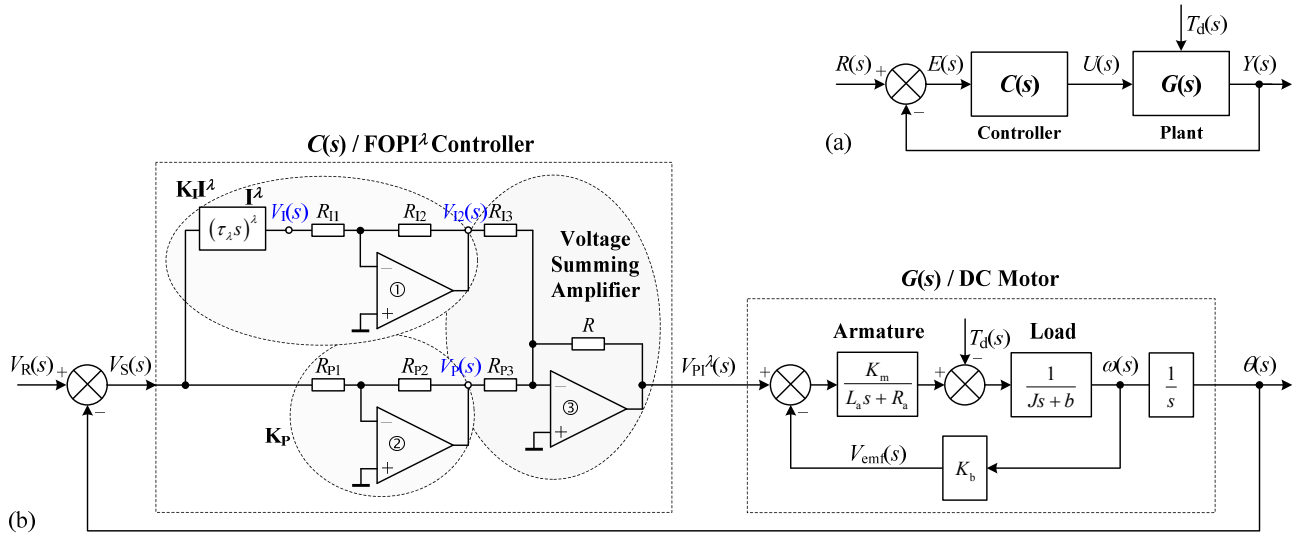

Fig. 2. (a) Block diagram of a control system, (b) an implementation of an analogue fractional-order PI$^\lambda$ controller and the mathematical model of a DC motor

controller can be advantageous for the speed and position control of an armature controlled DC motor without the requirement of its interfacing with computer [26], [27] for instance. The behavior of proposed integrator and controller was verified by AC and transient analyses via SPICE software.

The paper is organized as follows: Section II briefly describes preliminary considerations of a general control system and DC motor. Section III presents a new FOPI$^\lambda$ controller design. The simulation results are shown in Section IV, while the last section includes the conclusions.

II. Description of a Control System and Preliminary Considerations

A general block diagram of a single loop feedback control system is depicted in Fig. 2(a). Transfer function of the system can be expressed as [28]:

$$\frac{Y(s)}{R(s)} = \frac{C(s)G(s)}{1+C(s)G(s)}, \tag{1}$$

where $G(s)$ is a plant, $C(s)$ is a controller, $R(s)$ is a reference input signal, $Y(s)$ is an output signal, $T_d(s)$ is an external disturbance, $U(s)$ is a control signal, and $E(s)$ is an error signal, which is given by $E(s) = R(s) - Y(s)$.

An implementation of a control system used to control the speed and position of an armature controlled DC motor is shown in Fig. 2(b). The system is composed of the proposed analogue implementation of a FOPI$^\lambda$ controller ($C(s)$), while $G(s)$ is the mathematical model of a DC motor - the plant [26]. In brief, assuming the external disturbance, i.e., load torque $T_d(s)$ is zero, the transfer function (TF) of the motor speed control in s-domain can be expressed as [27]:

$$G(s) = \frac{\omega(s)}{V_{\mathrm{PI}^\lambda}(s)} = \frac{K_m}{(L_a s + R_a)(Js + b) + K_b K_m}, \tag{2}$$

where $V_{\mathrm{PI}}{}^\lambda(s)$ is the applied armature voltage, $\omega(s)$ is the angular velocity (controlled variable), L_a is an inductance of armature winding, R_a is an armature resistance, K_b is back-emf constant, K_m is a torque constant, and J is an equivalent moment of inertia and b is friction coefficient of motor and load referred to motor shaft. As the armature time constant for most of DC motors is negligible, the simplified TF of DC motors has the form $G(s) = K_{DC}/(\tau s + 1)$, where $\tau = R_a J/(R_a b + K_b K_m)$ is the time constant and $K_{DC} = K_m/(R_a b + K_b K_m)$ is the gain with $K_b = K_m$. Similarly, the TF for armature voltage and position $\theta(s)$ (controlled variable) will be $G_\theta(s) = K_{DC}/[s(\tau s + 1)]$.

III. A Proposed FOPI$^\lambda$ Controller Design

In control theory, the gain crossover frequency (ω_{cg}) implies that the modulus of the open-loop transfer function follows $|C(j\omega_{cg})G(j\omega_{cg})| = 1$ and phase margin (Φ_m) sets a condition upon the phase of the open-loop system at the ω_{cg}, which can be expressed as $\Phi_m = \arg[C(j\omega_{cg})G(j\omega_{cg})] + \pi$. Considering the setup [27], the TF of the DC motor voltage-speed with 25% break is:

$$G(s) = \frac{\omega(s)}{V_{\mathrm{PI}^\lambda}(s)} = \frac{0.25}{1.45s+1}, \tag{3}$$

while the performance specification is $\omega_{cg} = 1.5$ rad/s and $\Phi_m = 60$ degree.

The speed (3) of a DC motor can be controlled using FOPI$^\lambda$, which TF in general has a form:

$$C(s) = \frac{U(s)}{E(s)} = \frac{V_{\mathrm{PI}^\lambda}(s)}{V_S(s)} = K_P + K_I s^\lambda, \tag{4}$$

which corresponds in discrete domain to a TF as follows:

$$C(z^{-1}) = \frac{U(z^{-1})}{E(z^{-1})} = K_P + K_I \left[\omega\left(z^{-1}\right)\right]^\lambda. \tag{5}$$

Equations (4) and (5) indicate the following three parameters, which can be independently set:

(i) K_P is the proportional constant,

(ii) K_I is the integration constant,

(iii) λ ($-1 < \lambda < 0$) is the fractional order of an integrator in Laplace domain, while in discrete domain it is an arbitrary real number.

Following [27], the graphical method yields the solution for design parameters, which are $K_P = 1.37$, $K_I = 2.28$, and $\lambda = -0.89$. Thus, the FOPI$^\lambda$ controller is obtained as:

$$C(s) = \frac{U(s)}{E(s)} = \frac{V_{\mathrm{PI}^\lambda}(s)}{V_\mathrm{S}(s)} = 1.37 + 2.28 s^{-0.89}. \tag{6}$$

The FOPI$^\lambda$ controller shown in Fig. 2(b) requires presence of a precise I$^\lambda$ design. Block diagram of a proposed integrator by cascade connection of first-order BTSs and first-order low-pass filter (LPF) is depicted in Fig. 3 and can be expressed as:

$$K_{\mathrm{I}^\lambda}(s) = \frac{V_\mathrm{I}(s)}{V_\mathrm{S}(s)} = \frac{\prod_{i=1}^{m}(s - z_i)}{\prod_{j=1}^{n}(s - p_j)} = \left.\frac{\sum_{i=1}^{m} a_i s^i}{\sum_{j=1}^{n} b_j s^j}\right|_{z_i, p_j \in \Re}, \tag{7}$$

where m denotes total number of BTS needed for the design of constant phase block and $n = m + 1$ will be mathematical order of the final circuit due to use of an additional LPF. The usefulness of LPF is described below.

Proposed realization of BTS using two ideal Op-Amps (assuming open loop gain $A \to \infty$) and a set of passive components is shown in Fig. 4(a), while the non-inverting LPF is depicted in Fig. 4(b). Transfer function of each segments are:

$$K_{\mathrm{BTS}\_m}(s) = \frac{V_{\mathrm{BTS\_OUT}m}(s)}{V_{\mathrm{BTS\_IN}m}(s)} = \frac{s + \omega_{zm}}{s + \omega_{\mathrm{p}m}} = \frac{2sC_m + \left(R_\mathrm{b} \parallel R_{zm}\right)}{2sC_m + \left(R_\mathrm{b} \parallel R_{\mathrm{p}m}\right)}, \tag{8a}$$

$$K_\mathrm{LPF}(s) = \frac{V_{\mathrm{LPF\_OUT}}(s)}{V_{\mathrm{LPF\_IN}}(s)} = \frac{1}{s + \omega_{\mathrm{p}m+1}} = \frac{1}{sC_{\mathrm{p}m+1}R_{\mathrm{p}m+1} + 1}, \tag{8b}$$

hence, zero and pole frequencies are:

$$\omega_{zm} = \frac{R_\mathrm{b} \parallel R_{zm}}{2C_m}, \tag{9a}$$

$$\omega_{\mathrm{p}m} = \frac{R_\mathrm{b} \parallel R_{\mathrm{p}m}}{2C_m}, \tag{9a}$$

$$\omega_{\mathrm{p}m+1} = \frac{1}{C_{\mathrm{p}m+1}R_{\mathrm{p}m+1}}, \tag{9a}$$

and transfer zero and poles are adjustable by resistors R_{zm}, $R_{\mathrm{p}m}$, and $R_{\mathrm{p}m+1}$, respectively.

Now, TF of cascade of m BTS and LPF in our particular case as depicted in Fig. 3 can be expressed as:

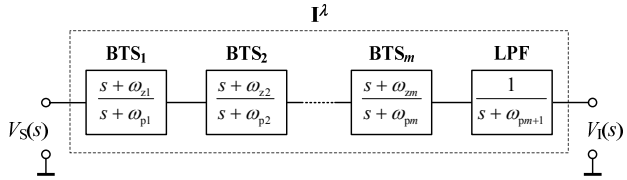

Fig. 3. Block diagram of a fractional-order integrator using BTSs and LPF

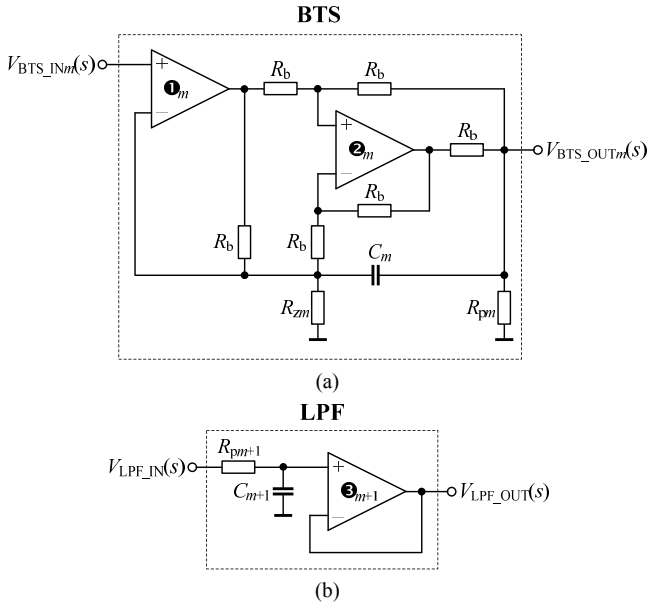

Fig. 4. (a) Realization of a bilinear transfer segment and (b) low-pass filter using Op-Amps

$$\begin{aligned} K_{\mathrm{I}^\lambda}(s) &= \frac{V_\mathrm{I}(s)}{V_\mathrm{S}(s)} = \\ &= K_{\mathrm{BTS}\_1}(s) K_{\mathrm{BTS}\_2}(s) \ldots K_{\mathrm{BTS}\_m}(s) K_\mathrm{LPF}(s) = \\ &= \prod_{i=1}^{m}\left[\frac{2sC_m + \left(R_\mathrm{b} \parallel R_{zm}\right)}{2sC_m + \left(R_\mathrm{b} \parallel R_{\mathrm{p}m}\right)}\right]\left(\frac{1}{sC_{\mathrm{p}m+1}R_{\mathrm{p}m+1} + 1}\right) = (\tau_\lambda s)^\lambda. \end{aligned} \tag{10}$$

Generalized TF (10) of a I$^\lambda$ has feature to set m pairs of zeros and poles independently and an additional pole as our design requires. The main advantage of this approach is an easy and low-cost realization of I$^\lambda$ using discrete passive components and on the shelf available Op-Amps.

Ones the I$^\lambda$ is designed, its integration constant K_I must be also realized. For this purpose the inverting Op-Amp configuration was selected, which closed loop voltage gain using an ideal Op-Amp can be calculated by ratio of two resistors in the path as $\mathrm{K_I} = -R_{\mathrm{I}2}/R_{\mathrm{I}1}$. The minus sign (–) comes from the inverting Op-Amp configuration and indicates a 180° phase shift. Now, the output voltage of the proposed fractional-order integrator with integration constant ($\mathrm{K_I I}^\lambda$) in time domain can be given as:

$$V_{\mathrm{I}2}(t) = -\frac{R_{\mathrm{I}2}\tau_\lambda^\lambda}{R_{\mathrm{I}1}} \int_0^t V_\mathrm{S}(t) dt^\lambda, \tag{11}$$

while in s-domain its TF is $-R_{I2}(\tau_\lambda s)^\lambda/R_{I1}$. Similarly, the inverting Op-Amp configuration was used also for proportional constant K_P realization and its output voltage is:

$$V_P(t) = -\frac{R_{P2}}{R_{P1}} V_S(t)\,. \tag{12}$$

Equations (4)–(6) indicate that a summing block is also required for FOPI$^\lambda$ design. In analogue electronics the Op-Amp-based summing amplifier is a suitable circuit for this purpose, which provides inverting weighted sum of input signals. Hence, the minus sign in (11) and (12) will be eliminated. Moreover, assuming the input resistors R and R_{P3} in Fig. 2(b) are equal, a unity gain adder will be added without affecting K_P and K_I constants. Finally, summing (11) and (12) as indicated in Fig. 2(b), the output voltage of the proposed FOPI$^\lambda$ in time domain will be:

$$\begin{aligned} V_{PI^\lambda}(t) &= -R\left[\frac{V_P(t)}{R_{P3}} + \frac{V_{I2}(t)}{R_{I3}}\right] = \\ &= R\left[\frac{R_{P2}}{R_{P1}R_{P3}} V_S(t) + \frac{R_{I2}\tau_\lambda^\lambda}{R_{I1}R_{I3}} \int_0^t V_S(t)dt^\lambda\right], \end{aligned} \tag{13}$$

and its equivalent transfer function in Laplace domain can be given as:

$$\begin{aligned} C(s) = \frac{U(s)}{E(s)} &= \frac{V_{PI^\lambda}(s)}{V_S(s)} = \\ &= K_P + K_I K_{I^\lambda}(s) = \\ &= R\left[\frac{R_{P2}}{R_{P1}R_{P3}} + \frac{R_{I2}(\tau_\lambda s)^\lambda}{R_{I1}R_{I3}}\right]. \end{aligned} \tag{14}$$

Comparing (4) and (14), the following design equations are derived:

$$K_P = \frac{RR_{P2}}{R_{P1}R_{P3}}, \quad K_I = \frac{R_{I2}\tau_\lambda^\lambda}{R_{I1}R_{I3}}, \tag{15a,b}$$

which will be useful in next section for FOPI$^\lambda$ design according to parameters as defined by (6).

IV. Simulation Results

To verify the theoretical analysis, the behavior of the proposed I$^\lambda$ and FOPI$^\lambda$ controller employing Op-Amps have been simulated by using SPICE program. DC power supply voltages of designed CMOS implementation of two-stage Miller compensated Op-Amp, shown in Fig. 5, were set $+V_{DD} = -V_{SS} = 0.9$ V. In [29], discrete components are assumed for both Miller resistor and load capacitor. The Op-Amp structure, shown in Fig. 5, is more favorable for full CMOS integration, because both components are realized via MOS-only technique, while the Miller capacitor can be realized as double poly (poly1-poly2) or metal-insulator-metal (MIM) capacitor. In the design, transistors were modeled by the TSMC 0.18 μm level-7 LO EPI SCN018 CMOS process parameters ($V_{THN} = 0.3725$ V, $\mu_N = 259.5304$ cm^2/(V·s), $V_{THP} = -0.3948$ V, $\mu_P = 109.9762$ cm^2/(V·s), $T_{OX} = 4.1$ nm). Following the design procedure described in [29], the computed aspect ratios of CMOS transistors and Op-Amp main parameters, which were obtained with DC, AC, and transient analyses, are listed in Table I and Table II, respectively. During all simulations the bias current in the structure was set as $I_B = 130$ μA.

TABLE I. Transistor Dimensions of Two-Stage Op-Amp in Fig. 5

PMOS Transistors	W (μm)/L (μm)
M_3, M_4	10.6 / 0.3
M_8	95.9 / 0.3
NMOS Transistors	**W (μm)/L (μm)**
M_1, M_2	25.8 / 0.3
M_5	15.4 / 0.3
M_6	16.4 / 0.3
M_7	58 / 0.3
M_R	4 / 0.3
M_C	288 / 3.6

TABLE II. Behavior of CMOS Two-Stage Op-Amp in Fig. 5

Parameter	Value	Unit
Power supply	±0.9	(V)
Unity gain bandwidth	230.2	(MHz)
DC gain	60	(dB)
Phase margin	60	(degree)
Slew rate +/–	163 / 121	(V/μs)
PSRR +/–	72.4 / 68.5	(dB)
CMRR	62.4	(dB)
Compensation resistor (NMOS M_R)	≅ 615	(Ω)
Compensation capacitor C_c	0.8	(pF)
Load capacitor (NMOS M_C)	≅ 3	(pF)
Power dissipation	1.39	(mW)
Total area	1 115.6	(μm^2)[#]

[#]Sum of products of widths and lengths of each transistors in the CMOS implementation

TABLE III. Computed Component Values Used in BTSs and LPF for Fractional-Order Integrator Design

Capacitors (F)					
C_1	C_2	C_3	C_4	C_5	C_6
27 μ	10 μ	12 m	68 μ	1.8 m	150 n
Resistors (Ω)					
R_b	R_{z1}	R_{z2}	R_{z3}	R_{z4}	R_{z5}
24 k	49	1.37 k	50.5 k	1.01 k	156
R_{p1}	R_{p2}	R_{p3}	R_{p4}	R_{p5}	R_{p6}
14 k	1 k	1.8 k	942	50.5 k	13 k

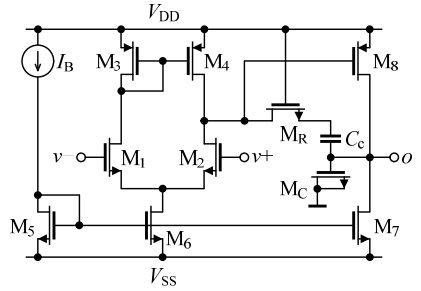

Fig. 5. CMOS structure of two-stage Op-Amp

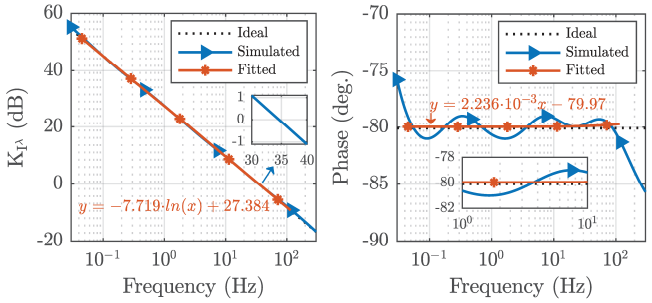

(a) (b)

Fig. 6. Ideal, simulated, and fitted (a) gain and (b) phase responses of 0.89-order integrator

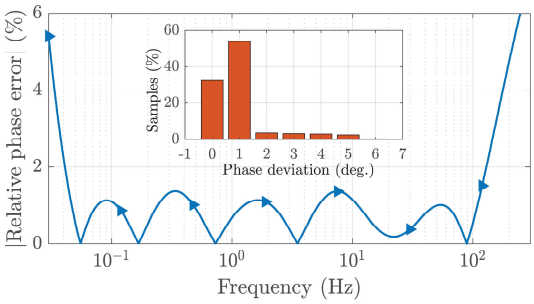

Fig. 7. Relative phase error and the corresponding normalized histogram for phase angle deviation evaluated in full frequency range

Firstly, the I^λ of order –0.89 (i.e. the time constant τ_λ^λ) was designed. The five-branch Valsa structure [21] was used, which provides a minimum phase angle deviation (PAD). Required R and C values were calculated via approach [25] implemented in Matlab with the following inputs: pseudo-capacitance $C_\lambda = 20\ \mu F \cdot sec^{-0.11}$, bandwidth (constant phase zone - CPZ) from 30 mHz up to 100 Hz (> 3 decades), constant phase angle (CPA) –80.1 degree (i.e. $\lambda = -0.89$), and PAD = ±1 degree. Preliminary calculations showed that five BTSs ($m = 5$) and a LPF are required in the constant phase block shown in Fig. 3 in order to achieve the design specification. Note that the LPF is used for correction purposes of additional pole in Valsa structure. As the next step, zero and pole frequencies were recalculated and corresponding passive component values of R_{zm}, R_{pm}, R_{pm+1}, C_m, and C_{pm+1} obtained via Matlab algorithm and optimized using modified least squares quadratic method. Component values used in BTSs and LPF for I^λ design are listed in Table III. Ideal and simulated gain and phase responses in frequency domain are given in Fig. 6. Selected zooms and equivalent equations for fitting the gain and phase in CPZ 45 mHz – 115 Hz via natural logarithm and linear regressions, respectively, are provided inside Figures. Simulated value of the unity-gain frequency of the I^λ was 34.6 Hz. As it can be seen in Fig. 7, in CPZ the maximum relative phase error is 1.38% and corresponding absolute PAD about 1 degree. Monte Carlo (statistical) analysis was performed with capacitors 5% tolerance, resistors 1% tolerance, and 200 runs to observe effects of deviations due to manufacturing processes. The histogram, shown in Fig. 8, demonstrates the variation of the phase of I^λ at 3 Hz. The mean value is –80.2389 degree, which is very close to theoretical value –80.1 degree, confirming that the proposed I^λ shows low

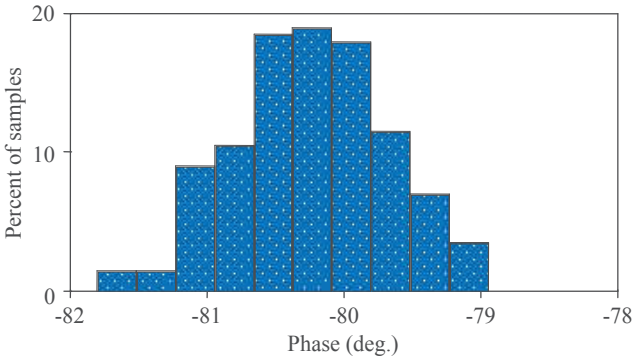


```
n samples    = 200          10th %ile = -81.0287
n divisions  = 10           median    = -80.2636
mean         = -80.2389     90th %ile = -79.4817
sigma        = 0.558949     maximum   = -78.9441
minimum      = -81.8069     3*sigma   = 1.67685
```

Fig. 8. Monte Carlo analysis: Variation of the phase of I^λ at 3 Hz

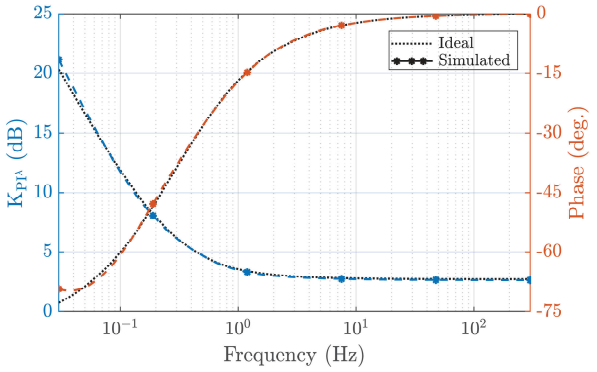

Fig. 9. Ideal and simulated gain and phase responses for the proposed $FOPI^\lambda$ controller

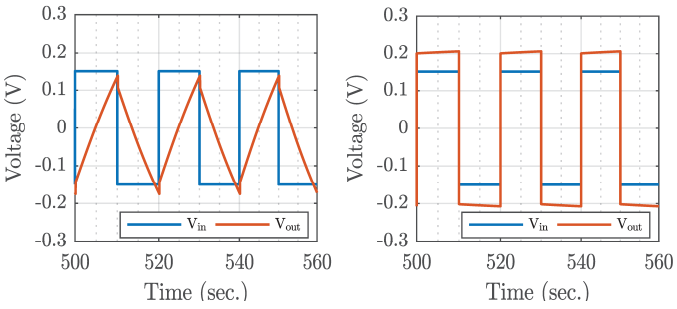

(a) (b)

Fig. 10. Time-domain responses of proposed (a) I^λ and (b) $FOPI^\lambda$ controller with applied square wave input voltage signal with frequency 100 mHz

sensitivity for deviations of passive components. Equation (6) indicates the following design parameters of the $FOPI^\lambda$ controller depicted in Fig. 2(b): $K_P = 1.37$, $K_I = 2.28$, and $\lambda = -0.89$. As the I^λ is designed, the remaining design parameters can be recalculated using (15), which are the following: $R = R_{P1} = R_{P3} = 10\ k\Omega$, $R_{P2} = 13.7\ k\Omega$, $R_{PI1} = 27.4\ k\Omega$, $R_{PI2} = 1.3\ k\Omega$, and $R_{PI3} = 24.9\ k\Omega$. An ideal and simulated gain and phase responses of the $FOPI^\lambda$ are given in Fig. 9. The results in the figure confirm the accurate operation of the controller. Moreover, in order to illustrate the time-

domain performance of I^{λ} and FOPI$^{\lambda}$ controller, transient analyses were performed, and results are depicted in Fig. 10. A square wave input signal with amplitude 150 mV and frequency 100 mHz with the following setup was applied to both circuits: $T_D = 0$, $T_R = 1$ ms, $T_F = 1$ ms, $T_{PW} = 10$ s, $T_{PER} = 20$ s, i.e., 12 time constants τ_{λ}^{λ}. Hence, complying with the theory of fractional calculus, in Fig. 10(a) the simulated output signal of the I^{λ} has triangular waveform, while Fig. 10(b) indicates increasing gain in the proposed FOPI$^{\lambda}$ controller as the effect of the K_P. From obtained results it can be seen that it is in very close agreement with the theory proving good performance of propose I^{λ} and FOPI$^{\lambda}$ controller.

V. Conclusion

The paper proposed an analogue realization of a I^{λ} and FOPI$^{\lambda}$ controller based on design specification corresponding to a speed control system of an armature controlled DC motor. The main advantage of this approach is an easy and low-cost realization using discrete components. For the I^{λ}, SPICE simulations using two-stage CMOS Op-Amps showed an absolute phase angle deviation about 1 degree in constant phase zone from 45 mHz to 115 Hz. Statistical analysis proved its low sensitivity characteristic for passive components. Simulated gain and phase responses of the FOPI$^{\lambda}$ confirmed accurate operation of the controller.

References

[1] J. Tenreiro-Machado, A. M. Lopes, D. Valério, and A. M. Galhano, *Solved Problems in Dynamical Systems and Control*. The IET, 2016.

[2] C. Yeroglu and N. Tan, "Note on fractional-order proportional-integral-differential controller design," *IET Control Theory & Applications*, vol. 5, no. 17, pp. 1978–1989, 2011.

[3] A. Dumlu and K. Erenturk, "Trajectory Tracking Control for a 3-DOF Parallel Manipulator Using Fractional-Order PI$^{\lambda}$D$^{\mu}$ Control," *IEEE Transactions on Industrial Electronics*, vol. 61, no. 7, pp. 3417–3426, 2014.

[4] A. A. Dastjerdi, N. Saikumar, and S. H. HosseinNia, "Tuning guidelines for fractional order PID controllers: Rules of thumb," *Mechatronics*, vol. 56, pp. 26–36, 2018.

[5] B. B. Alagoz, "Fractional order linear time invariant system stabilization by brute-force search," *Transactions of the Institute of Measurement and Control*, vol. 40, no. 5, 1447–1456, 2018.

[6] P. Ko and M. Tsai, "H∞ Control Design of PID-Like Controller for Speed Drive Systems," *IEEE Access*, vol. 6, pp. 36711-36722, 2018.

[7] H. Ren, J. Fan, and O. Kaynak, "Optimal Design of a Fractional-Order Proportional-Integer-Differential Controller for a Pneumatic Position Servo System," *IEEE Transactions on Industrial Electronics*, vol. 66, no. 8, pp. 6220–6229, 2019.

[8] S. Razvarz, C. Vargas-Jarillo, R. Jafari, and A. Gegov, "Flow Control of Fluid in Pipelines Using PID Controller," *IEEE Access*, vol. 7, pp. 25673-25680, 2019.

[9] A. Tepljakov, B. B. Alagoz, C. Yeroglu, E. Gonzalez, S. H. HosseinNia, and E. Petlenkov, "FOPID controllers and their industrial applications: a survey of recent results," *IFAC-PapersOnLine*, vol. 51, pp. 25–30, 2018.

[10] R. Magin, B. Vinagre, and I. Podlubny, "Can Cybernetics and Fractional Calculus Be Partners?: Searching for New Ways to Solve Complex Problems," *IEEE Systems, Man, and Cybernetics Magazine*, vol. 4, no. 3, pp. 23–28, 2018.

[11] I. Podlubny, B. Vinagre, P. O'leary, and L. Dorcak, "Analogue realizations of fractional-order controllers," *Nonlinear Dynamics*, vol. 29, pp. 281–296, 2002.

[12] A. Charef, "Analogue realisation of fractional-order integrator, differentiator and fractional PI$^{\lambda}$D$^{\mu}$ controller," *IEE Proceedings - Control Theory and Applications*, vol. 153, no. 6, pp. 714–720, 2006.

[13] D. Sierociuk, I. Podlubny, and I. Petras, "Experimental Evidence of Variable-Order Behavior of Ladders and Nested Ladders," *IEEE Transactions on Control Systems Technology*, vol. 21, no. 2, pp. 459–466, 2013.

[14] H. Nezzari, A. Charef, and D. Boucherma, "Analog Circuit Implementation of Fractional Order Damped Sine and Cosine Functions," *IEEE Journal on Emerging and Selected Topics in Circuits and Systems*, vol. 3, no. 3, pp. 386–393, 2013.

[15] K. Biswas, G. Bohannan, R. Caponetto, A. M. Lopes, and J. A. T. Machado, *Fractional-Order Devices*. Springer, 2017.

[16] A. K. Gilmutdinov, P. A. Ushakov, and R. El-Khazali, *Fractal Elements and their Applications*. Springer, 2017.

[17] A. M. Elshurafa, M. N. Almadhoun, K. N. Salama, and H. N. Alshareef, "Microscale electrostatic fractional capacitors using reduced graphene oxide percolated polymer composites," *Applied Physics Letters*, vol. 102, pp. 232901–232904, 2013.

[18] A. Kartci, A. Agambayev, A. H. Hassan, H. Bagci, and K. N. Salama, "Experimental Verification of a Fractional-Order Wien Oscillator Built Using Solid-State Capacitors," In *Proc. of 2018 IEEE 61st International Midwest Symposium on Circuits and Systems (MWSCAS)*, Windsor, ON, Canada, 2018, pp. 544-545.

[19] A. Kartci, A. Agambayev, N. Herencsar, and K. N. Salama, "Series-, parallel-, and inter-connection of solid-state arbitrary fractional-order capacitors: theoretical study and experimental verification," *IEEE Access*, vol. 6, pp. 10933–10943, 2018.

[20] D. A. John, S. Banerjee, G. W. Bohannan, and K. Biswas, "Solid-state fractional capacitor using MWCNT-epoxy nanocomposite," *Applied Physics Letters*, vol. 110, 163504, 2017.

[21] J. Valsa, P. Dvorak, and M. Friedl, "Network model of the CPE," *Radioengineering*, vol. 20, pp. 619–626, 2011.

[22] G. Tsirimokou, A. Kartci, J. Koton, N. Herencsar, and C. Psychalinos, "Comparative study of discrete component realizations of fractional-order capacitor and inductor active emulators," *Journal of Circuits Systems and Computers*, vol. 27, no. 11, pp. 1850170-1–1850170-26, 2018.

[23] J. Petrzela, "Fundamental analog cells for fractional-order two-port synthesis," In *Proc. of 23rd Conference Radioelektronika*, Czech Republic, 2013, pp. 182–187.

[24] R. Sotner, J. Jerabek, N. Herencsar, J. Petrzela, T. Dostal, and K. Vrba, "First-order adjustable transfer sections for synthesis suitable for special purposes in constant phase block approximation," *AEU - International Journal of Electronics and Communications*, vol. 69, pp. 1334–1345, 2015.

[25] R. Sotner, J. Jerabek, A. Kartci, O. Domansky, N. Herencsar, V. Kledrowetz, B. B. Alagoz, and C. Yeroglu, "Electronically Reconfigurable Two-Path Fractional-Order PI/D Controller Employing Constant Phase Blocks Based on Bilinear Segments Using CMOS Modified Current Differencing Unit," *Microelectronics Journal*, vol. 86, pp. 114-129, 2019.

[26] I. Petras, "Fractional-Order feedback control of a DC motor," *Journal of Electrical Engineering*, vol. 60, no. 3, pp. 117–128, 2009.

[27] C. Copot, C. I . Muresan, and R. De Keyser, "Speed and position control of a DC motor using fractional order PI-PD control," In *Proc. of 3rd Int. Conference on Fractional Signals and Systems*, Ghent, Belgium, 2013, pp. 1–6.

[28] B. B. Alagoz, A. Tepljakov, C. Yeroglu, E. Gonzalez, S. H. HosseinNia, and E. Petlenkov, "A numerical study for plant-independent evaluation of fractional-order PID controller performance," *IFAC-PapersOnLine*, vol. 51, pp. 539–544, 2018.

[29] Y. Guo, "An accurate design approach for two-stage CMOS operational amplifiers," In *Proc. of IEEE Asia Pacific Conf. on Circuits and Systems (APCCAS)*, Jeju, Korea, 2016, pp. 563–566.